Synthesis of a tunable ring filter: Proof-of-concept with fixed implementations at D-band

Pedro Rynkiewicz, Anne-Laure Franc, Fabio Coccetti, Matthias Wietstruck, Mehmet Kaynak, Gaëtan Prigent

Synthesis of a tunable ring filter: Proof-of-concept with fixed implementations at D-band

Authors : Pedro Rynkiewicz, Anne-Laure Franc, Fabio Coccetti, Matthias Wietstruck, Mehmet Kaynak, and Gaëtan Prigent

Affiliations :
- P. Rynkiewicz was with the LAPLACE, University of Toulouse, CNRS, INPT, UPS, Toulouse, France.
- A.-L. Franc is with the LAPLACE, University of Toulouse, CNRS, INPT, UPS, Toulouse, France (anne-laure.franc@laplace.univ-tlse.fr).
- F. Coccetti is with the IRT Saint Exupéry, Toulouse, France
- M. Wietstruck and M. Kaynak are with IHP, Im Technologiepark 25, 15236 Frankfurt (Oder), Germany.
- Gaëtan Prigent is with LAAS-CNRS, Université de Toulouse, CNRS, Toulouse, France.

Data Availability Statement : The data that support the findings of this study are available from the corresponding author upon reasonable request.

Abstract : The working frequencies of telecommunication systems is rapidly increasing and sub-THz applications will soon be required. In that context, the current article presents the synthesis of a tunable ring filter. The considered filter introduces a new degree of freedom that allows to meet targeted specifications in terms of central frequency and bandwidth. Thanks to a capacitor displacement, the equivalent characteristic impedance can be tuned independently of its equivalent electrical length. The existing filter synthesis is modified to take this concept into account and thus provide a synthesis tunable in central frequency and bandwidth. The proof-of-concept of the design procedure is achieved in SiGe BiCMOS 0.25µm technology with the implementation and measurement of 8 non-tunable circuits in the D-band.

Keywords : Filter synthesis, integrated circuits, capacitive loading, frequency and bandwidth control

I. Introduction

Current and future communication systems require transceivers dealing with many standards. So, a whole transceiver is comprised of similar electronic parts differing only in their center frequencies or their bandwidths [1]. Thus, there is a need of easy-to-design tunable circuits to reach compact systems at reasonable costs.

Besides, due to the data rate increase, high frequency systems are targeted [2]. Many results are already available for the 5G application in the V-band but few circuits have been presented in the sub-THz which will be useful for backhauling links as the atmospheric attenuation exhibits a minimum around 140 GHz [3]. In this context, silicon technologies are interesting to reach low-cost systems at high frequencies but the losses remain the main problem. Therefore, studies have to be carried out on passive circuits. In the state-of-the-art, most filters in D-band are realized either in substrate integrated technologies [4]-[6] or with BCB [7] or GaAs [8] technologies and few results exist in integrated silicon technologies [9]-[10].

In the literature, many methods are considered to achieve tunable filters with independent control of the center frequency and bandwidth. The tunability can be achieved with the control of electrical lengths [11]-[13]. In [11] the cascade connection of two tunable filters (one low-pass, one high-pass) leads to a bandpass tunable filter. In [12] and [13], a topology based on parallel stubs is used to tune the transmission zeros frequencies, thus modifying the center frequency and bandwidth of the filter. If the chosen topology is based on resonators, it is possible to tune the filter by adjusting the coupling between them [14] or the mode resonance frequencies for multimode resonators [15]-[16]. Some topologies exhibit the possibility to vary simultaneously the electrical lengths and the coupling also leading to tune-all bandpass filters [17]-[19].

The fully reconfigurable filters of this state-of-the art are demonstrated below the millimeter-wave frequency range and most of them are working at RF frequencies. The latter require varactors while the higher frequency circuits use MEMS elements to achieve the tuning. Among them, [12], [14], [16], [18] are based on a synthesis which is crucial for an efficient design step.

The current paper introduces a tunable filter synthesis relying on capacitors displacement along a ring resonator (see [20] for the fixed frequency synthesis). The principle of a capacitor displacement has already been used in [21] around 2 GHz: A varactor connected in series inside a resonator leads to reconfigurable bandpass filters with predefined tuning range depending on the position of the varactors. The current paper presents a solution with parallel placed capacitors which are easier to implement.

This paper is organized as follows. Section II firstly presents a quarter-wavelength transmission line that exhibits a tunable equivalent impedance when varying the position of a capacitive load. Then, the loaded transmission line is introduced in the ring resonator topology to demonstrate a bandwidth control with the capacitor position. Finally, the full synthesis is provided. Section III validates this synthesis with the implementation in SiGe BiCMOS 0.25 µm technology at sub-THz. The limited performance of tuning elements in the D-band did not allow to realize efficient tunable devices and the independent control of the center frequencies and bandwidths is demonstrated with the measurement of various fixed-frequency filters. Section IV shows a benchmark of D- and G-band filters. Finally, the conclusion summarizes the main results and gives some perspectives of this work.

II. Theory

As the paper focuses on tunability, two specific frequencies are defined: f_{high} and f_{low} for the high- and low-frequency states respectively.

A. Transmission line loaded with two varying position capacitors

To allow a fine tuning of a loaded transmission line characteristics, the concept of the capacitors displacement along the line is introduced and this new degree of freedom is theoretically studied. As

depicted in Fig. 1, a transmission line is loaded by two capacitors symmetrically located in relation to its center. Z_c and θ_h are the characteristic impedance and electrical length of the non-loaded transmission line. The position of the capacitors along the line is represented thanks to a real number *P* between 0 and 1: When *P* is set to 0 both capacitors overlap in the center and for *P*=1 the capacitors are placed at both sides of the transmission line. Thereby, the electrical lengths θ_P and $\theta_{1\text{-}P}$ are defined as a function of θ_h:

$$\theta_P = P \cdot \frac{\theta_h}{2}\,, \qquad (1)$$

$$\theta_{1-P} = (1-P) \cdot \frac{\theta_h}{2}. \qquad (2)$$

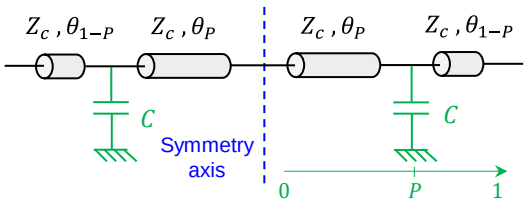

Fig. 1. Transmission line loaded with two symmetrically connected displaceable capacitors.

This loaded transmission line behaves like an equivalent one with Z_{eq} and ϑ_{eq} its equivalent characteristic impedance and electrical length. For future implementation in the filter, the unloaded transmission line must be a quarter-wavelength at the high frequency (θ_h=90° at f_{high}) and the capacitances should be correctly chosen so as to reach a quarter-wavelength at a lower frequency (θ_{eq}=θ_l=90° at f_{low}). To determine the required capacitances *C*, the chain matrix of the loaded transmission line has been calculated by cascading the four transmission line elements with the two parallel capacitors. At f_{low}, the transmission line is supposed to be quarter-wavelength, thus, in the lossless case, the final chain matrix is (3).

$$\begin{pmatrix} A_{cascade} & B_{cascade} \\ C_{cascade} & D_{cascade} \end{pmatrix} = \begin{pmatrix} 0 & jZ_{eq} \\ jY_{eq} & 0 \end{pmatrix} \qquad (3)$$

Hence by solving $A_{cascade} = 0$, a quadratic equation appears with the normalized capacitance $C_N = 2\pi f_{low} Z_C C$ as unknown. Two solutions exist and (4) is the one that allows to get a zero capacitance if no frequency shift is targeted (*i.e.,* θ_{eq}=90° at f_{high}).

$$C_N = \frac{\sin\theta_h - \cos\theta_h \sqrt{2\sin^2 P\theta_h + \tan^2\theta_h - \sin 2P\theta_h \tan\theta_h}}{\sin\theta_h \sin P\theta_h \cos P\theta_h - \cos\theta_h \sin^2 P\theta_h} \qquad (4)$$

Then, the equivalent impedance value can be calculated as (5). Figure 2 shows the equivalent impedance continuous variation versus the capacitor position *P*. For this graph, Z_c (which is a degree of freedom for the designer) is set to 50 Ω and f_{high} to 155 GHz. The capacitances are calculated to target θ_{eq} = 90° at three different frequencies for f_{low}, namely 145 GHz, 135 GHz and 125 GHz. In this specific case, the equivalent characteristic impedance at the low frequency 135 GHz continuously varies between 40.8 Ω and 49 Ω when *P* increases from 0 to 1.

$$Z_{eq} = \sqrt{\frac{B_{cascade}}{C_{cascade}}} = Z_c \sqrt{\frac{2\sin\theta_h + 2C_N(\cos\theta_h - \cos P\theta_h) + {C_N}^2 \sin P\theta_h sin^2(1-P)\theta_h/2}{2\sin\theta_h + 2C_N(\cos\theta_h + \cos P\theta_h) - {C_N}^2 \sin P\theta_h cos^2(1-P)\theta_h/2}} \qquad (5)$$

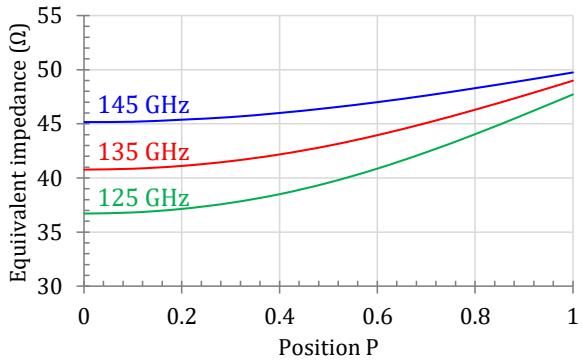

Fig. 2. Equivalent impedance as a function of P for f_{low} = 145, 135 and 125 GHz (f_{high}=155 GHz, Z_c=50 Ω).

Finally, the choice of the capacitor position allows a control of the equivalent impedance at f_{low} keeping electrical lengths equal to 90° at f_{high} (unloaded) and f_{low} (loaded). It is of great interest in the field of tunable components as it realizes impedance inverters with a tunable characteristic impedance.

B. Fully tunable ring filter

In this subsection, a fully tunable ring filter topology concept is presented. A first topology that implements the aforementioned principle is shown. A second one combines the impedance variation principle with the loaded ring filter presented in [20].

1) Empirical study

The loaded transmission line detailed in the previous part is implemented in each arm of the symmetric filter topology (Fig. 3). Note that the same normalized capacitor is used for vertical and horizontal arms but since two characteristic impedances (Z_1, Z_2) are used, two capacitor values (C_{a1}, C_{a2}) are finally required.

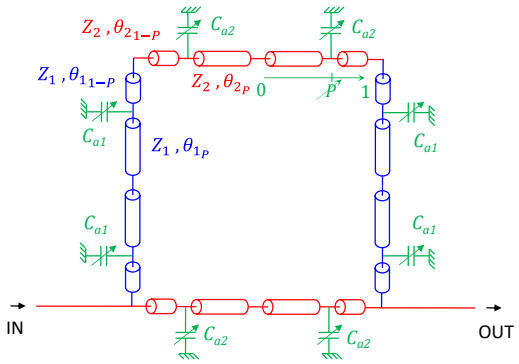

Fig. 3. Schematic of the first tunable filter topology.

As the unloaded transmission line is a quarter-wavelength at f_{high} and the capacitances calculation forces the loaded transmission line equivalent electrical length to 90° at f_{low}, the filter necessarily reaches the two targeted center frequencies (f_{high}, f_{low}). Moreover, the capacitors displacement leads to characteristic impedance modification, thus the bandwidth is modified with *P*.

Nevertheless, the return loss being explicitly set by the impedance values [20], the low frequency matching cannot be controlled this way. Keeping the symmetry, it has been observed that a reasonable capacitor imbalance while maintaining a constant value for the sum of the capacitances allows to keep the same low frequency. Thus, the modification of the equivalent impedances is realized with the

introduction of a compensation capacitor C_{comp}: C_{comp} is added to C_{a1} and subtracted to C_{a2}. Eventually, as C_{a1} is replaced by C_{a1}+C_{comp} and C_{a2} by C_{a2}-C_{comp}, the impedance ratio between the vertical and horizontal arms is monitored with the C_{comp} value, thus modifying the matching at the low frequency. For a selected 20-dB matching level, the position of the capacitors controls the bandwidth as shown in Fig. 4.

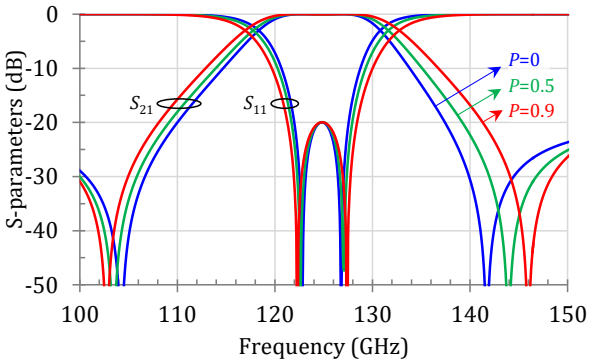

Fig. 4. Bandwidth variation of the low frequency state with the capacitors position P (f_{high}=155GHz, f_z=126GHz, y=20dB; f_{low}=125GHz).

However, when P is equal to 1, C_{a1}+C_{comp} and C_{a2}-C_{comp} overlap in the corners and the final value of the capacitors do no longer depend on C_{comp}. To overcome this issue, the proposed solution is to choose a high frequency design with a very deep matching level (*e.g.* 60 dB) and limit the low frequency to an acceptable matching value (*e.g.* 20 dB) when P=1.

2) Miniaturization advantage and calculation

In this part, a capacitance C_m is added in the center of each arm (Fig. 5). The calculation of Z_{ci} and ϑ_{ci} are given in [20].

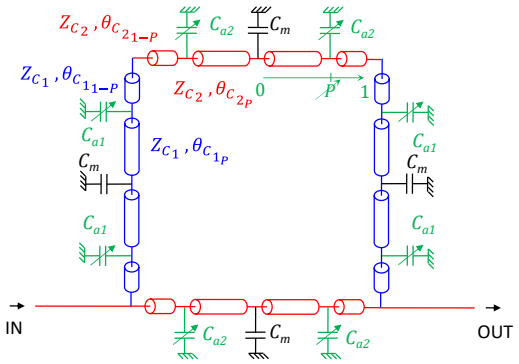

Fig. 5. Schematic of the miniaturized tunable ring topology.

Besides the conventional advantages of the loading (miniaturization, increase in the nominal characteristic impedances), all the observations realized without the miniaturization capacitors remain the same and the achievable bandwidth range at the low frequency is increased with the miniaturized topology, Fig. 6.

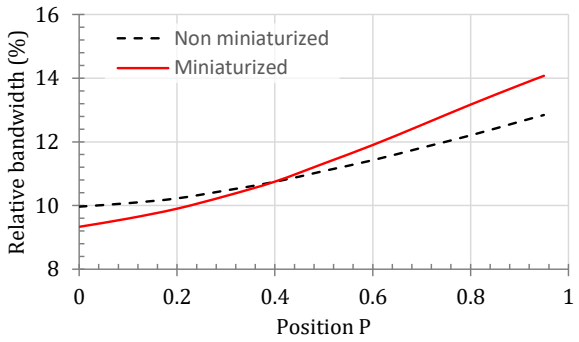

Fig. 6. Bandwidth variation with the capacitors position P for a constant 20 dB matching (f_{high}=155GHz, f_z=126GHz, y=20dB; f_{low}=125GHz).

The last step to supply a resonator synthesis with tunable center frequency and bandwidth is to provide the calculation of the compensation capacitance C_{comp}. Several abaci have been considered to determine this value in the general case. The normalized compensation capacitance $C_{comp\_n} = 2\pi f_{high} \cdot C_{comp} \cdot Z_0$ (with Z_0 = 50 Ω) is plotted versus various parameters (Figs. 7-9).

Figure 7 shows the normalized compensation capacitance that is required to reach at each capacitance position *P* the same matching level than the non-controllable one for *P*=1. This graph, obtained for various frequency shifts, exhibits a small compensation variation along *P* for low frequency shifts. Moreover, keeping a constant return loss is not necessary if the matching remains good enough. Thereby, to simplify the filter design, a constant compensation capacitance obtained for *P*=0 is considered in the following. If the frequency shift is limited to 20%, the matching level remains reasonably low (around 20 dB in the worst case) wherever the capacitors are placed, even for *P*=1 which is the worst case as mentioned before.

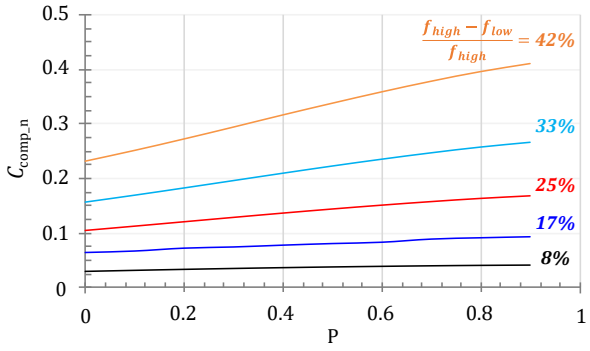

Fig. 7. Normalized compensation capacitance versus the position P for various frequency shifts.

Figure 8 gives the normalized compensation capacitance evolution versus the frequency shift for several low-frequency transmission zero values, f_z (related to the high frequency state). It is obvious that the bandwidth impacts the compensation capacitance value which can be considered as linear towards the frequency shift.

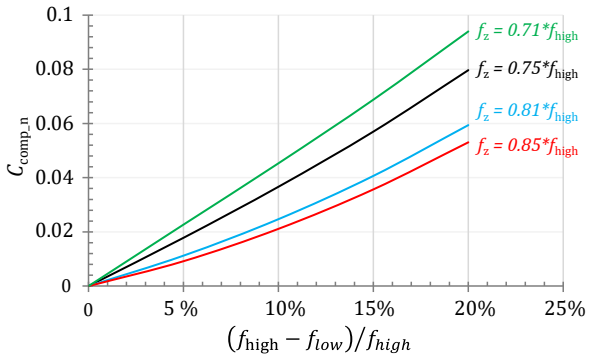

Fig. 8. Normalized compensation capacitance versus the frequency shift for various first transmission zero frequencies. (C_{comp_n} is chosen to ensure that the matching level at P=0 is equal to its value at P=1.)

Then, the normalized compensation capacitance is plotted in Fig. 9 versus the low-frequency transmission zero (corresponding to the high frequency state). This graph is obtained for a 20% frequency shift which corresponds to the reference value for the linear approximation of C_{comp_n}. Note that the transmission zero is normalized with the high frequency value. A linear approximation can be used for bandwidths ranging between 8% and 30%. The associated slope from simulations is $\frac{C_{comp\_n}|30\%}{f_{z\_n}|30\%} = \frac{1}{3}$.

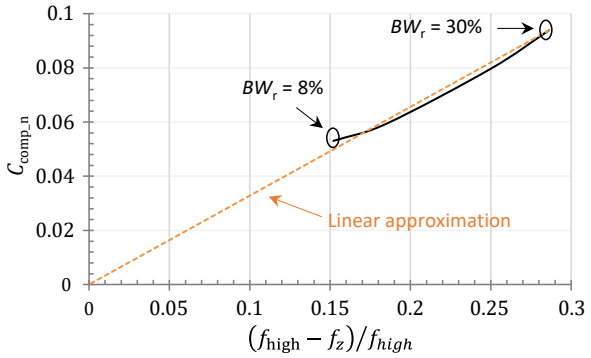

Fig. 9. Normalized compensation capacitance versus the high frequency state first transmission zero for a 20% frequency shift and the same matching level at P=0 and P=1.

Eventually, the normalized compensation capacitance is approximated with (6).

$$C_{comp\_n} \cong \frac{1}{3} \cdot \frac{f_{high} - f_z}{f_{high}} \cdot \frac{f_{high} - f_{low}}{f_{high}} \qquad (6)$$

3) Conclusion

Based on previous studies, a synthesis is available for a ring resonator with two independent tunable parameters (center frequency and bandwidth). The design procedure is the following. Considering that the high frequency state is realized fixing Z_{c1} and the matching level equal to 50 Ω and 60dB respectively, the designer chooses the center frequency f_{high}, low-transmission zero f_z and [20] imposes the miniaturization capacitance C_m, it gives us the impedance Z_{c2} and the electrical lengths θ_{c1}, θ_{c2}. Then, the initial capacitances C_{a1} and C_{a2} are calculated thanks to (4) to reach the targeted low center frequency f_{low} (any value of P can be considered). If the bandwidth does not meet the requirements, then the position P of the capacitors is modified and C_{a1} and C_{a2} are recalculated accordingly. Eventually the compensation capacitance C_{comp} is computed with (6) and the final values of the capacitors are C_{a1}+C_{comp} and C_{a2}-C_{comp}.

This calculation has a specific validity domain: *i)* the starting point is a miniaturized ring with Z_{c1} = 50 Ω and a 60 dB matching level, *ii)* a frequency shift lower than 20%, and *iii)* a relative 3-dB fractional bandwidth at high-frequency between 8% and 30%.

III. D-band filters implementation

This synthesis has been used for filter implementation in the CMOS 0.25 µm technology provided by the IHP foundry. The back-end-of-line exhibits five metal layers and MIM capacitors are available, Fig. 10 and in [22]. All the measurements presented in this section have been realized with the setup of Fig. 11 after a conventional TRL deembedding step.

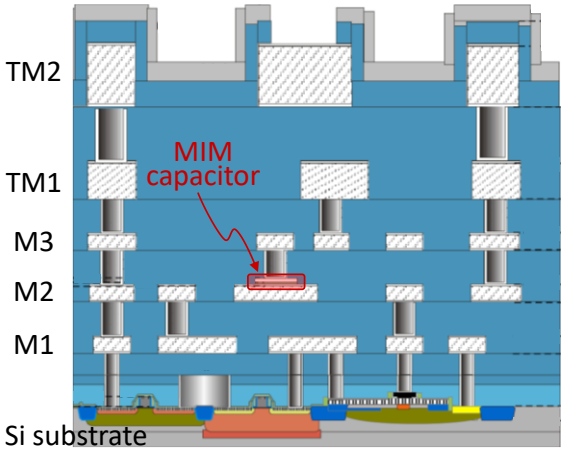

Fig. 10. IHP 0.25µm BiCMOS 0.25µm cross-section.

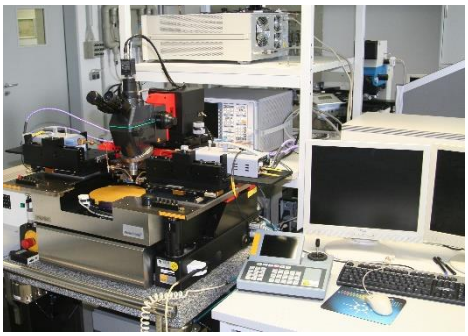

Fig. 11. IHP's measurement setup.

For the proof-of-concept, various non-tunable devices have been realized and tested separately. A microstrip transmission line topology has been chosen with the signal conductor on the top metal layer and a massive ground plane on the bottom one.

A. High frequency cell

The equations of [20] have been used to design the high frequency cell with a center frequency f_{high}=155 GHz, a 12% 3-dB fractional bandwidth and a matching level of 60 dB at f_{high}. The electrical parameters are the following: Z_{c1}=50 Ω, ϑ_{c1}=22.7° at f_{high}, Z_{c2}=29.6 Ω, ϑ_{c2}=29.9° at f_{high} and C_m=C_1=C_2=40.4 fF. Fig. 12 shows a photography of the device that is composed of four transmission lines, each of them being loaded with a capacitor (C_1 or C_2) in its center for a miniaturization purpose (no position varying capacitor).

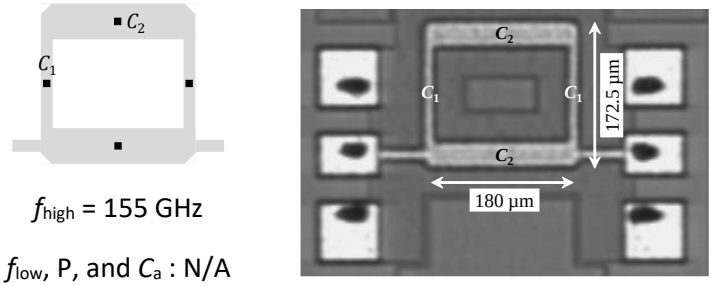

Fig. 12. (a) Layout representation and (b) photography of the 155 GHz ring filter.

A particularly good agreement is obtained between the initial electromagnetic simulation (without any post-simulation) and the measurement results (Fig. 13) confirming that the non-tunable synthesis leads to the targeted properties. A 11.5% fractional bandwidth is measured, the insertion loss is 4.5 dB and the matching level is better than 40 dB at the center frequency.

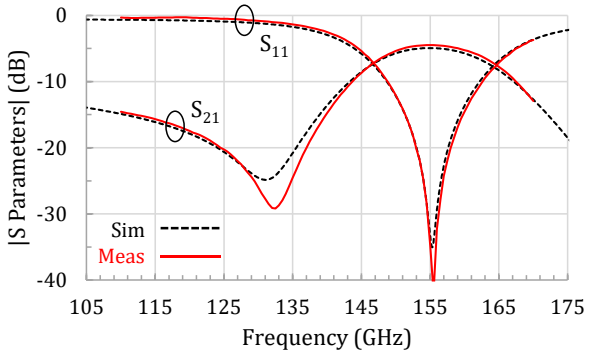

Fig.13. Simulation and measurement results of the high-frequency cell.

B. Tunability proof-of-concept

This subsection aims at demonstrating the potential tunability based on the theory developed above. In the following, all the filters are based on the previous 155-GHz filter and they differ only in the size and position of their MIM capacitors used for tunability (C_{a1}, C_{a2} including their needed compensation) which are below the signal strip and thus not visible. So, all the devices look like the high frequency filter of Fig.12 and layout representations are used in the following.

1) Bandwidth tuning

As explained in the theoretical part, the equivalent characteristic impedance controls the bandwidth of ring filters and this impedance value can be modified, independently from the equivalent electrical length at f_{low}, by changing both the position and the value of the C_a capacitors.

Here, a filter is realized to characterize the achievable bandwidth shift for a 135 GHz center frequency (f_{low}). The layouts and main electrical properties are given in Fig. 14. It appears that precise and low C_a values are required to realize the correct bandwidth with good return loss. This is not a problem in integrated technologies as the size of the capacitors can be adjusted to reach specific values. One should note that the C_{a1} and C_{a2} numerical values directly include the compensation capacitances.

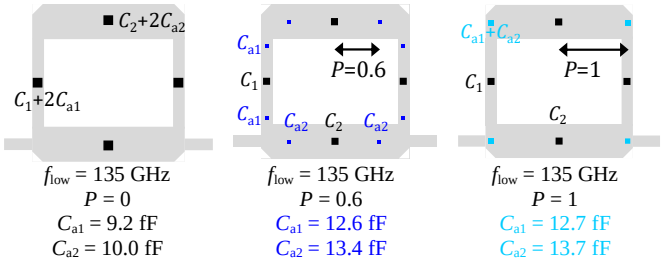

Fig. 14. Layout representations of 3 ring resonators for bandwidth tuning at 135 GHz.

Fig. 15 shows the deembedded S-parameters for four filters with the capacitor position *P* between 0 and 1. They clearly highlight that the capacitor position variation modifies the bandwidth. Thereby, a filter with a high-frequency state at 155 GHz with an 18.3 GHz bandwidth can lead to a low-frequency state at 135 GHz with a bandwidth between 15.2 GHz and 19 GHz, corresponding to a 22% variation. The other electric results are good as the return loss remains better than 20 dB at the center frequencies and the insertion loss achieves values between 3.7 dB and 4.7 dB for the high- and low-frequency states.

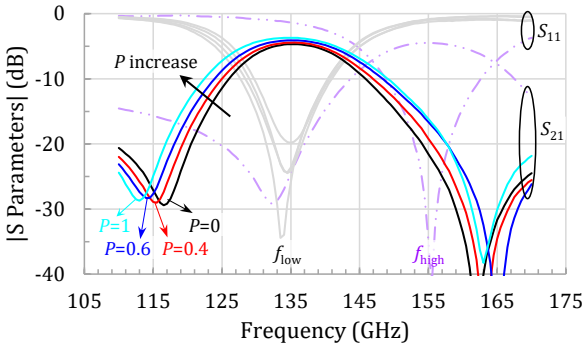

Fig. 15. Measurement of the high-frequency and low-frequency states. The latter being tunable in bandwidth when the C_{a1} and C_{a2} capacitor position and value vary.

2) Center frequency tuning

In this subsection, the center frequency is tuned between 145- and 125-GHz while keeping a constant bandwidth.

a) Constant absolute bandwidth

The synthesis is applied to design three filters at different center frequencies keeping the same 17-GHz bandwidth, Fig. 16.

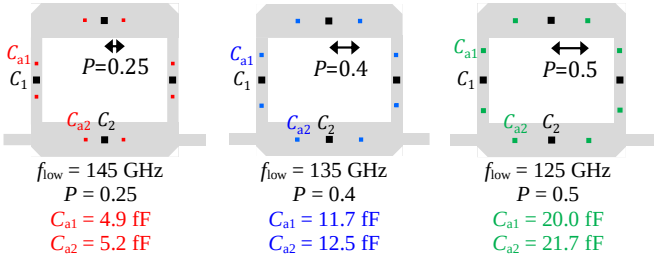

Fig. 16. Layout representations of the ring resonators having the same 17-GHz natural bandwidth.

The measurement results are compared with the simulations in Fig. 17. The very good agreement confirms that the tunable synthesis is reliable and allows center frequency tuning while keeping a constant bandwidth. The measured 3-dB absolute bandwidth ranges from 16 GHz to 16.8 GHz, *i.e.,* less

than 5% variation. To confirm this, a translation of the center frequency has been applied and leads to Fig. 18.

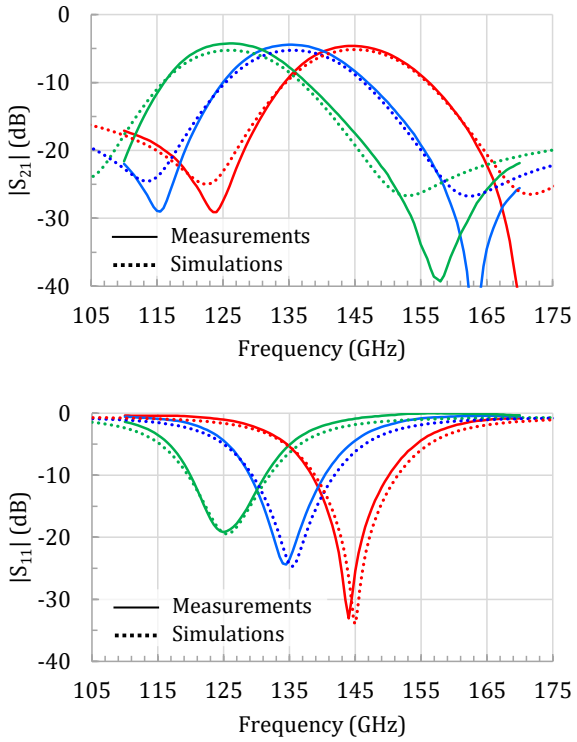

Fig. 17. S-parameters of the three filters having a 17-GHz natural bandwidth.

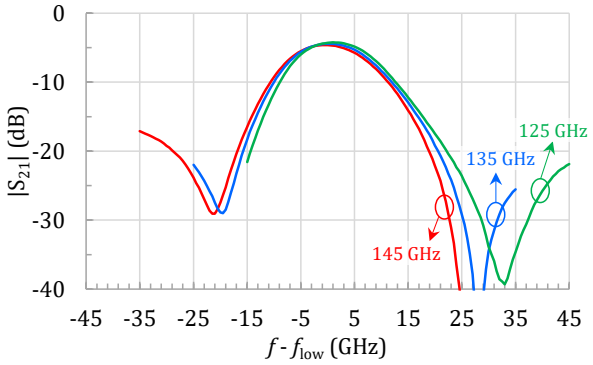

Fig. 18. Natural bandwidth comparison of the measured circuits.

b) Constant relative bandwidth

In a similar way, a tuned filter can provide a constant fractional bandwidth at its various center frequencies. The next results show a 13.5% 3-dB bandwidth at 145 GHz (f_{low}=145GHz, P=0.7, C_{a1}=6.1fF, C_{a2}=6.3fF), 135 GHz (f_{low}=135GHz, P=0.6, C_{a1}=12.6fF, C_{a2}=13.4fF) and 125 GHz (f_{low}=125GHz, P=0.5, C_{a1}=20.0fF, C_{a1}=21.7fF).

The deembedded results are displayed in Fig. 19 with the associated simulations. Figure 20 shows the measurement results versus the normalized frequency. So, the synthesis allows to easily implement filters with a large frequency tuning range (20 GHz) while keeping a constant fractional bandwidth (here between 12.7% and 13.4%, *i.e.,* a 5% variation). Besides, a correct matching level (better than 19 dB) is obtained for reasonable insertion losses (less than 4.2 dB).

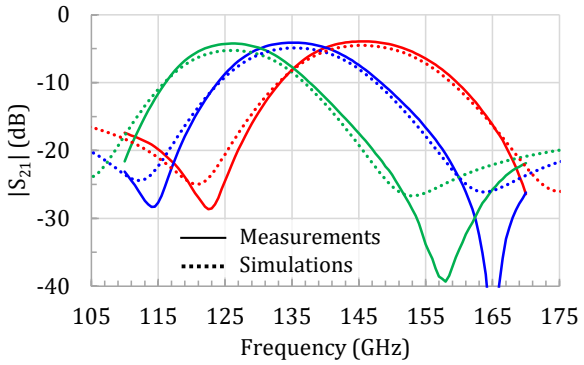

Fig. 19. Transmission parameters for a constant fractional bandwidth.

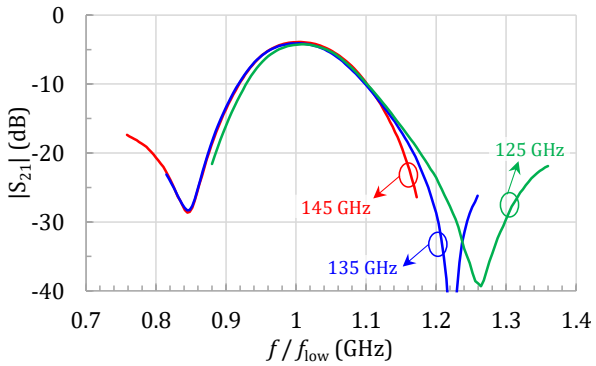

Fig. 20. Comparison of the fractional bandwidth.

C. Conclusion on the measurements

The frequency-fixed results discussed in this section highlight the high potentiality of the tunable synthesis. Hence an important center frequency shift has been demonstrated in keeping similar absolute or relative bandwidth. Naturally, it is also possible to target two independent working states: two different center frequencies and two different bandwidths. The limitations are the dynamic of the achievable bandwidth, which increase with the frequency shift, and the return loss level that deteriorates when increasing the frequency shift.

Moreover, the synthesis, design process and technology are fully reliable as no post-simulation has been needed to correctly predict the circuits' behavior.

IV. Benchmark

Table I presents a state-of-the-art for integrated planar filters at D- and G-band. An approximation of the unloaded quality factor Q_u is given for each filter based on equation (7) with n the filter order, BW_{r_3dB} the relative bandwidth and IL_{dB} the insertion loss, [23].

$$Q_u = 4.343 \cdot \frac{n}{\mathrm{BW}_{r\_3dB} \cdot IL_{dB}} \qquad (7)$$

[8] and [9] describe stub-based third-order filters implemented on GaAs or HRSOI (High Resistive Silicon On Insulator)Due to the chosen topology, the electric responses display a wide bandwidth. Similar results are presented in [7], where a second-order filter is realized with stepped impedance

resonators. Those three filters display low insertion loss (thanks to their wide bandwidth) and the required surface areas are quite important. [10] shows a 2nd order 24% 3_{dB}-fractional bandwidth combline filter in a CMOS 0.13 µm technology. Thus, the comparison with the current paper is easier. On the one hand, [10] is more compact than the here-proposed solution and has less insertion loss explained by a larger bandwidth and a better conductor (copper instead of aluminum). On the other hand, the current paper shows a reasonable compact filter topology that allows to envision full tunable devices.

Table I. State-of-the-art for D-band and G-band planar filters

Techno.	f_c	BW_{r_3dB}	BW_{a_3dB}	IL	RL	Q_u	Area		Ref.		
GaAs	165 GHz	57%	94 GHz	1.33 dB	18 dB	17.2	0.2 mm²	$0.06\cdot\lambda_0^2$	[8]		
HRSOI	170 GHz	40%	68 GHz	2.3 dB	20 dB	14.2	N/A		[9]		
BCB on Si	136 GHz	32.2%	43.8 GHz	2.94 dB	10 dB	9.2	0.4 mm²	$0.08\cdot\lambda_0^2$	[7]		
0.13 µm CMOS	170 GHz	24%	40 GHz	2.7 dB	17 dB	13.4	0.004 mm²	$0.0013\cdot\lambda_0^2$	[10]		
0.25µm BiCMOS	155 GHz	11.8%	18.3 GHz	4.5 dB	42 dB	16.4	0.031 mm²	between $0.0055\cdot\lambda_0^2$ and $0.008\cdot\lambda_0^2$	f_{high}		This work
	146 GHz	13.4%	19.5 GHz	3.9 dB	27 dB	16.6			f_{low}	P=0.7	
	144 GHz	11.6%	16.8 GHz	4.6 dB	33 dB	16.3				P=0.25	
	135 GHz	14.1%	19 GHz	3.7 dB	33 dB	16.6				P=1	
	136 GHz	13.1%	17.8 GHz	4.1 dB	24 dB	16.2				P=0.6	
	136 GHz	12.2%	16.5 GHz	4.1 dB	23 dB	17.4				P=0.4	
	136 GHz	11.2%	15.2 GHz	4.7 dB	20 dB	16.5				P=0	
	126 GHz	12.7%	16 GHz	4.2 dB	19 dB	16.3				P=0.5	

V. Conclusion

This paper introduces impedance inverters working at two different frequencies with a controllable tunable characteristic impedance for the low frequency. The tuning is realized by the displacement of capacitors along the transmission line. This elementary cell can be implemented in future for many tunable circuits, like tunable inverters for instance.

Based on this concept, a synthesis is given for a tune-all ring filter. Within a given validity domain, it is theoretically possible to choose two working frequencies and independently set each bandwidth. For a proof-of-concept of the design procedure, various non-tunable circuits have been measured at D-band. They exhibit both the bandwidth variation as well as the possibility to target constant bandwidths for different frequency shift values.

This work paves the way of a fully tunable filter. A fully tunable implementation would require several switched capacitors but the losses of integrated switches are still a limitation to get high performance circuits in the D-band.

Acknowledgement

The authors would like to thank Selin Tolunay Wipf, Christian Wipf and Barbaros Cetindogan, IHP (Germany), for their valuable assistance.

References

[1] G. M. Rebeiz, K. Entesari, I. C. Reines, S.-J. Park, M. A. Eltanani, A. Grichener, R. Brown. Tuning in to RF MEMS. IEEE Microwave magazine 2009; 10 (6): 55-72.

[2] M. J. Marcus. 5G and "IMT for 2020 and beyond" [Spectrum Policy and Regulatory Issues]. IEEE Wireless Communications 2015; 22 (4): 2-3.
[3] J. Wells. Faster than fiber: The future of multi-G/s wireless. IEEE Microwave Magazine 2009; 10 (3), pp. 104-112.
[4] F. David, C. Dalmay, M. Chatras, A. Pothier, L. Carpentier, L. Lapierre, P. Blondy. 3D micro-fabricated high-Q 140 GHz filter. International Microwave Symposium Honololu HI United States. 4-9 June 2017.
[5] K. Wang, S. Wong, G. Sun, Z. N. Chen, L. Zhu, Q. Chu. Synthesis Method for Substrate-Integrated Waveguide Bandpass Filter With Even-Order Chebyshev Response. IEEE Transactions on Components, Packaging and Manufacturing Technology 2016; 6 (1): 126-135.
[6] W. Cheng, L. Bin, L. Jie, D. Xianjin. 140GHz waveguide H ladder bandpass filter. International Conference on Microwave and Millimeter Wave Technology Shenzhen China. 5-8 May 2012.
[7] R. Li, T. G. Lim, S. W. Ho, Y. Z. Xiong, Y. M. Khoo. Wideband bandpass filter design for D-band application. IEEE Electrical Design of Advanced Package & Systems Symposium Singapore. 7-9 Dec. 2010.
[8] G. Wolf, G. Prigent, E. Rius, S. Demichel, R. Leblanc, G. Dambrine, H. Happy. Band-pass coplanar filters in the G-frequency band. IEEE Microwave and Wireless Components Letters 2005; 15 (11): 99-801.
[9] F. Gianesello, D. Gloria, S. Montusclat, C. Raynaud, S. Boret, G. Dambrine, S. Lepillier, B. Martineau, R. Pilard. 1.8 dB insertion loss 200 GHz CPW band pass filter integrated in HR SOI CMOS Technology. International Microwave Symposium Honolulu HI United States. 3-8 June 2007.
[10] X. Wang, H. S. Wu, C. K. C. Tyuang. CMOS 170 GHZ combline bandpass filter. IEEE International Conference on Microwaves for Intelligent Mobility Heidelberg Germany. 27-29 Apr. 2015.
[11] B. Pillans, A. Malczewski, R. Allison, J. Brank. 6-15 GHz RF MEMS tunable filters. IEEE International Microwave Symposium Long Beach CA United States. 17 June 2005.
[12] E. Fourn, C. Quendo, E. Rius, A. Pothier, P. Blondy, C. Champeaux, J.C. Orlianges, A. Catherinot, G. Tanne, C. Person, F. Huret. Bandwidth and central frequency control on tunable bandpass filter by using MEMS cantilevers. IEEE MTT-S International Microwave Symposium Philadelphia PA United States. 8-13 June 2003.
[13] K. Kawai, H. Okazaki, S. Narahashi. Ring resonators for bandwidth and center frequency tunable filter. European Microwave Conference Munich Germany. 9-12 Oct. 2007.
[14] P. W. Wong and I. C. Hunter. Electronically Reconfigurable Microwave Bandpass Filter. IEEE Transactions on Microwave Theory and Techniques 2009; 57 (12): 3070-3079.
[15] A. L. C. Serrano, F. S. Correra, T. Vuong P. Ferrari. Synthesis Methodology Applied to a Tunable Patch Filter With Independent Frequency and Bandwidth Control. IEEE Transactions on Microwave Theory and Techniques 2012; 60 (3): 484-493.
[16] D. Lu, X. Tang, N. S. Barker, M. Li, T. Yan. Synthesis-Applied Highly Selective Tunable Dual-Mode BPF With Element-Variable Coupling Matrix. IEEE Transactions on Microwave Theory and Techniques 2018; 66 (4): 1804-1816.
[17] D. Mercier, J.-C. Orlianges, T. Delage, C. Champeaux, A. Catherinot, D. Cros, P. Blondy. Millimeter-wave tune-all bandpass filters. IEEE Transactions on Microwave Theory and Techniques 2004; 52 (4): 1175-1181.
[18] E. Pistono, M. Robert, L. Duvillaret, J.-M. Duchamp, A. Vilcot, P. Ferrari. Compact fixed and tune-all bandpass filters based on coupled slow-wave resonators. IEEE Transactions on Microwave Theory and Techniques 2006; 54 (6): 2790-2799.
[19] G. Zhang, Y. Xu, X. Wang. Compact Tunable Bandpass Filter With Wide Tuning Range of Centre Frequency and Bandwidth Using Short Coupled Lines. IEEE Access 2018; 6: 2962-2969.
[20] P. Rynkiewicz, A.-L. Franc, F. Coccetti, M. Wietstruck, M. Kaynak, G. Prigent. Ring filter synthesis and its BiCMOS 60-GHz implementation. International Journal of Microwave and Wireless Technologies 2018; 10 (3): 291-300.

[21] D. Lu, X. Tang, N. S. Barker, Y. Feng. Single-Band and Switchable Dual-/Single-Band Tunable BPFs With Predefined Tuning Range, Bandwidth, and Selectivity. IEEE Transactions on Microwave Theory and Techniques 2018; 66 (3): 1215-1227.
[22] P. Rynkiewicz, A.-L. Franc, F. Coccetti, M. Wietstruck, M. Kaynak, G. Prigent. A compact millimeter-wave dual-mode ring filter using loaded capacitances in CMOS 0.25µm technology. International Microwave Symposium San Francisco CA United States. 22-27 May 2016.
[23] G. L. Matthaei, L. Young, E. M. T. Jones. Microwave filters, impedance-matching networks, and coupling structures, Norwood, MA: Artech House; 1980.